Sensors & Actuators: B. Chemical 370 (2022) 132482

Contents lists available at ScienceDirect

Sensors and Actuators: B. Chemical

journal homepage: www.elsevier.com/locate/snb

Resistive type NO_2 gas sensing in polymer-dispersed liquid crystals with functionalized-carbon nanotubes dopant at room temperature

Srinivas Pagidi [a,b], Kedhareswara Sairam Pasupuleti [a], Maddaka Reddeppa [b], Soyeon Ahn [a], Youngseo Kim [a], Jong-Hyun Kim [a,b], Moon-Deock Kim [a,b], Seung Hee Lee [c,*], Min Yong Jeon [a,b,**]

[a] Department of Physics, Chungnam National University, 99 Daehak-ro, Yuseong-gu, Daejeon 34134, the Republic of Korea
[b] Institute of Quantum Systems (IQS), Chungnam National University, 99 Daehak-ro, Yuseong-gu, Daejeon 34134, the Republic of Korea
[c] Department of Nano Convergence Engineering and Department of Polymer-Nano Science and Technology, Jeonbuk National University, Jeonju, Jeonbuk 54896, the Republic of Korea

ARTICLE INFO

Keywords:
Liquid crystal
PDLC
Functionalized-carbon nanotube
NO_2 gas
Sensor

ABSTRACT

The embedding of liquid crystal (LC) droplets into polymer matrices yields polymer-dispersed liquid crystals (PDLCs), which play an important role in the formation of mechanically resistant films for flexible photonic devices. Despite the fact that PDLCs respond to a variety of physical and chemical stimuli, LCs have had limited success in detecting environmental pollutants due to a lack of reactive functional groups in their structures. In this work, we execute the idea of integrating functionalized carbon nanotubes (f-CNTs) into PDLCs to accelerate the absorption of gas molecules at room temperature (RT). The proposed f-CNT-PDLC sensor device was prepared by depositing the composite mixture onto an interdigitated electrode substrate and carrying out phase separation under UV light exposure. Compared to the pure PDLC device, the proposed device exhibited a response of ~12.9 % and 1 % for 100 and 5 ppm of NO_2 gas, and a linear relationship was obtained with gas concentrations. Furthermore, this device displayed a good reproducibility over five cycles, exhibiting an excellent selectivity against other interfering gases, such as H_2S, CO, H_2, and NH_3. The boosted response was attributed to charge transport between the NO_2 gas molecules and the f-CNTs, which was detected by measuring the change in electrical resistance caused by the f-CNTs, in addition to the orientational phase modulation of the f-CNTs and the LCs within a droplet. Our experimental results revealed that the proposed f-CNT-doped PDLCs are promising candidates for sensing various physical and chemical stimuli.

1. Introduction

Gas sensing technology is one of the most important technologies in the context of environmental protection and the detection of pollutants that are harmful to the human health. Over the last few decades, metal oxide semiconductor (MOS) and conductive polymers have played a significant role in the precise detection of a wide range of toxic gases, and many fruitful efforts have been made to enhance their selectivities, responses, and response and recovery times at room temperature (RT). Despite these remarkable advantages, gas sensor technologies based on these materials employ a power supply because they require elevated temperatures to operate effectively, that falls far short of real time device applications. Besides, these can be fabricated usually on rigid substrates i.e., Silicon (Si) wafer, ceramic and glass [1–5]. On the other hand, liquid crystals (LCs) have been widely utilized in display and tunable photonic systems over the last few decades [6–9]; however, their application in the fields of bio- and gas sensors has received little attention. From this perspective, contemporary research interest has focused predominantly on LCs due to their facile tunability and nanoscale self-assembly properties, which permit both in situ and real-time gas sensing. In addition, LC-based gas sensing technologies have been shown to offer fast response and recovery times, even at RT [10,11], and they are also portable due to their low cost, light weight, and compact size [12]. Upon exposure to a target gas or specific biological environment, the orientation of LC molecules is interrupted, thereby rendering them applicable in the detection of biological- and gas-based stimuli. However, conventional LC sensors are also extremely sensitive to external mechanical stimuli, such as bending or pressure, and their

* Corresponding author.
** Corresponding author at: Department of Physics, Chungnam National University, 99 Daehak-ro, Yuseong-gu, Daejeon 34134, the Republic of Korea.
E-mail addresses: lsh1@jbnu.ac.kr (S.H. Lee), myjeon@cnu.ac.kr (M.Y. Jeon).

https://doi.org/10.1016/j.snb.2022.132482
Received 2 April 2022; Received in revised form 27 June 2022; Accepted 3 August 2022
Available online 5 August 2022

surface areas can be significantly deformed when the gas flow rate is excessively high, which renders them unsuitable for use in flexible sensors [11,13]. More recently, polymer-dispersed liquid crystal (PDLC) films have emerged as one of the most promising materials for integration with flexible substrates since they provide mechanical stability and can avoid the LC flow associated with external pressure application. Surprisingly, PDLCs pave the way for overcoming the inherent difficulties of conventional gas sensing devices that are based on the use of fluid nematic LCs [14,15]. In addition, they have been shown to detect gas molecules at RT with no mechanical deformation of the sensor film as the gas flow rate increases.

To produce PDLCs, nematic LCs are initially combined with photocurable monomers prior to phase-separation under ambient temperature conditions using the well-known polymerization-induced phase separation (PIPS) process [16,17]. As a result, the fluid nematic LC droplets are confined three-dimensionally in a transparent cross-linking polymer matrix that provides additional mechanical support to the LC molecules, which can lead to invariant optical and electrical properties in either the bending or twisting mode. Thus, the PDLC material can be easily deposited on a single glass or plastic substrate to yield a soft and mechanically stable film [15,16]. Furthermore, upon the application of an external stimulus, the optical changes resulting from variation in the LC droplet orientation can be easily visualized by polarized optical microscopy (POM) owing to the optical birefringence of the LCs.

PDLCs have been considered as potential candidates for application in a variety of fields, such as smart windows, optical phase modulators, flat panel displays, artificial iris, and fiber-optic electric field sensors [18,19]. In addition, a number of PDLC-based gas sensors have been reported to date, including PDLCs containing dispersed carbon nanotubes (CNTs) for the detection of dimethyl methylphosphonate (DMMP) [20]. In addition, a selection of PDLC composites have demonstrated excellent performances in the sensing of volatile organic compounds (VOCs) when prepared using CNTs (for the detection of acetone) [15] and zinc oxide (ZnO) nanorods (for the detection of ethanol) [21,22]. Although such systems have potential for the detection of VOCs, very few studies have been published in relation to the photonic sensing of environmentally hazardous gases. As one example, LCs doped with chiral binaphthyl-diamine dopants and LCs supported on gold surfaces have been shown to exhibit NO_2 gas detection properties [23,24]. Moreover, although CNTs have been considered as promising candidates for gas sensor applications owing to their unique structure, large specific surface area, high conductivity, and hollow geometry [25–28], the gas sensing properties of pure CNTs are limited owing to their low response and poor selectivity. To address this issue, we considered the functionalization of CNTs with surface OH groups.

Thus, in the present proof-of-concept study, the surface functionalization of commercially available single-walled carbon nanotubes (SWCNTs or f-CNTs) is performed by acid treatment to improve their dispersion in an LC medium [29,30], and subsequently, the as-prepared f-CNTs are mixed with a homogeneous mixture of LCs and photocurable monomers to prepare the proposed composite. Exposure of this composite to UV light is then carried out to generate the desired f-CNT-doped PDLCs (f-CNT-PDLCs), and the application of the prepared f-CNT-PDLC sensor in the detection of NO_2 gas is investigated at RT for the first time. It is hypothesized that the interaction of NO_2 gas molecules with the f-CNTs will result in a change in the f-CNT orientation, which in turn should modify the LC configuration within the droplet. Finally, a resistive gas sensing system is used to determine how the gas sensing responses change with respect to the NO_2 gas concentration (5–100 ppm). It is expected that our results will pave the way for the development of next-generation wearable gas sensing devices.

2. Material and methods

2.1. The f-CNT-PDLC gas sensing mechanism

A schematic representation of the proposed f-CNT-PDLC device for NO_2 gas sensing is shown in Fig. 1. The f-CNT-PDLC sensor device was fabricated over a single substrate with interdigitated electrodes, as shown in Fig. 1(a). The sensor device is composed of micrometer-sized LC droplets embedded in a continuous polymer matrix, and doped f-CNTs are dispersed both throughout the polymer matrix and within the encapsulated droplets. Usually, the fully submerged f-CNTs within the droplets mostly follow the long-range order of the LC director owing to the strong surface interaction between them and their orientation of f-CNTs and the LC molecules within the droplet remains constant in the field-off state ($E = 0$), [29,31,32]. On the other hand, when the electric fields ($E < E_{th}$) are applied between the interdigitated electrodes, the f-CNTs and LC molecules tend to align parallel to the substrate [33] because the LC molecules with a positive dielectric anisotropy ($\Delta\varepsilon$) are strongly anchored to the f-CNT surface, as shown in Fig. 1(b). This condition refers to the initial resistance (R_a) of the f-CNT-PDLC sensor device. The electrical conductivity measurement of the sensor device is favored for estimating quantitative data because the conductivity anisotropy is dominated by the conducting path distribution along various directions [34].

In this context, the NO_2 gas molecules absorb and undergo physisorption onto the sensor surface prior to diffusing and interacting directly with the f-CNTs in the film in the presence of NO_2 atmosphere, because of f-CNT's high surface area, abundant functional groups, and active surface sites. The surface-attached NO_2 gas molecules, which are strong oxidizing agents, can then react with these active sites to extract the free electrons (e^-) from the conduction band of the f-CNTs due to its high electronegativity, resulting in the generation of NO_2^- and NO_3^- ions. The following equations outline the induced surface reactions that result from the presence of NO_2 gas molecules:

$$NO_2(gas) + e^- \rightarrow NO^-_{2(ads)} \quad (1)$$

$$NO_2(gas) + O^-_{2(ads)} \rightarrow NO_2^- + O_2 \quad (2)$$

$$2NO_2(gas) + O^-_{2(ads)} + e^- \rightarrow 2NO_3^- \quad (3)$$

It was found that upon the introduction of NO_2 gas molecules, the ordering of the f-CNTs and the LC molecules was disturbed because the surface absorbed O_2 molecules seize the e^- that disturb the conductive path distribution of f-CNTs which in turn altered the orientational transition of the LC phase within the droplet away from the preferred phase to give the isotropic phase [29]. The restructured orientational phase of the droplet shown in Fig. 1(c) that reduces the mobility of charge carriers in the sensor device owing to the electron-acceptor charge transfer between the f-CNTs and the NO_2 gas molecules [35,36]. As a result, the charge carrier concentration in the conduction band of the f-CNTs decreases significantly, resulting in an increase in the resistance (R_g) of the f-CNT-PDLC sensor under NO_2 gas ambient. In this context, the sensor response (R) of the f-CNT-PDLC can be estimated using the equation [37,38],

$$R(\%) = \frac{(R_g - R_a)}{R_a} \times 100 = \frac{\Delta R}{R_a}, \quad (4)$$

where R_g and R_a represent the electrical resistance upon exposure to the target NO_2 gas and to air, respectively.

2.2. Materials

In the present experiment, the commercially available LC, E7, which is a mixture of 4-pentyl-40-cyanobiphenyl (51 %), 4-heptyl-40-cyanobiphenyl (25 %), 4-octyloxy-40-cyanobiphenyl (16 %), and 4-pentyl-40-

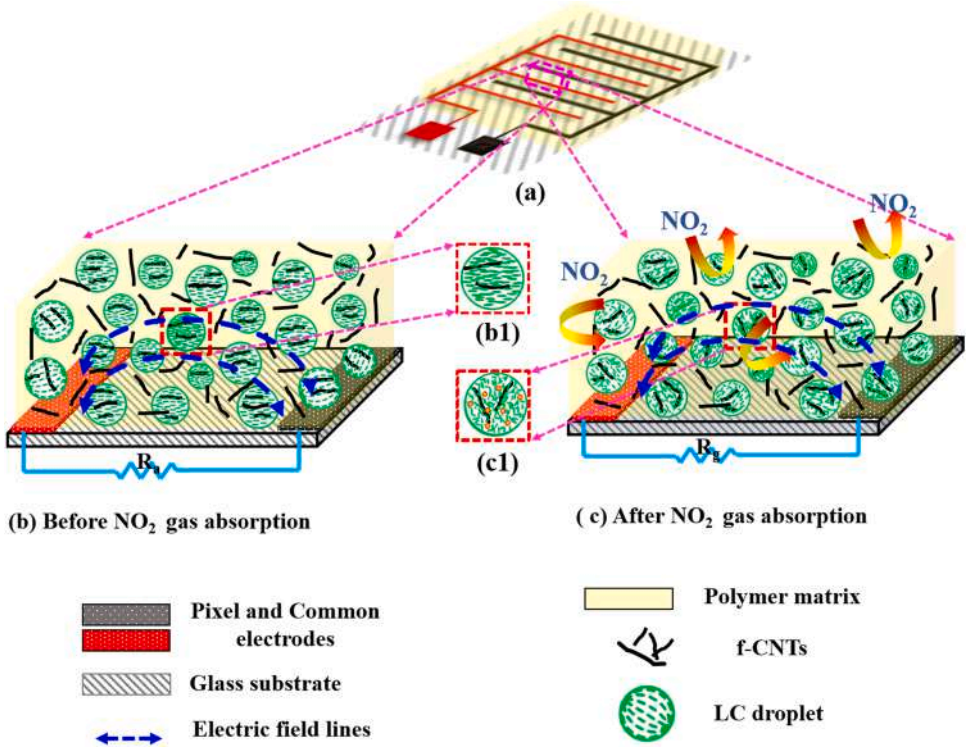

Fig. 1. Schematic representation of the f-CNT-PDLC gas sensor: (a) The fabricated f-CNT-PDLC sensing device, (b) orientations of the LCs and the f-CNTs in the absence of NO_2 gas, and (c) restructured LCs and f-CNTs in response to NO_2 gas inside the droplet, at $E < E_{th}$. The corresponding enlargements are shown in parts (b1) and (c1).

cyanobiphenyl (8 %) with a dielectric anisotropy Δε of 14.1 at 1 kHz, a birefringence Δn of 0.217 at 589 nm, and clearing temperature T_{NI} of 68 °C (Merck Advanced Technology, Korea), was used as the nematic LC. The molecular structures of the E7 LC were presented in Fig. S1. Norland optical adhesive (NOA-65), which is a thiol-ene-based prepolymer composed of a mixture of trimethylolpropanetris thiol (42 wt. %), trimethylopropane diallyl ether (3 wt. %), isophorone diisocyanate ester (54 wt. %), and benzophenone (1 wt. %, a photoinitiator (PI)), was used as the prepolymer and had a refractive index n_p of 1.5122 at 20 °C and 589 nm. The NOA-65 prepolymer absorbs UV light in the wavelength range of 350–380 nm. A small amount of Irgacure-651 (Irg-651, a PI) was added to the LC and prepolymer mixture to enhance the radical polymerization rate upon UV light exposure. Commercially available conductive SWCNTs (Avention Co., Korea) were used as dopants to absorb the target gas molecules.

2.3. Acidification process

SWCNTs with a diameter of 1.1 nm and a length of 1–3 μm were utilized for the purpose of our investigations. The large pristine SWCNTs form agglomerations in highly viscous prepolymer owing to their stronger van der Waals forces. For this reason, an acidification process was conducted to functionalize the surfaces of the SWCNTs and to reduce their size by inhibiting the formation of agglomerations. In order to obtain this, the pristine SWCNTs (5 mg) were dispersed in a concentrated mixture of H_2SO_4 and HNO_3 (3:1 (v/v), 2.5 mL), and the mixture was subjected to ultrasonication for 3 h to produce a homogeneous mixture. Subsequently, this mixture was washed several times with double-distilled water and centrifuged at 12,000 rpm for 25 min to neutralize the solute. The resultant mixture was dried in a vacuum oven at 150 °C for 2 h to remove any traces of solvent or water. Finally, the obtained f-CNT powder was thoroughly dispersed in acetone by ultrasonication for 30 min [29,30]. The length distribution of the prepared f-CNTs ranged from 120 to 620 nm, with a mean value of ~290 nm, as previously demonstrated by dynamic light scattering (DLS) [30].

2.4. Sample preparation

The pure PDLC sample was prepared using a mixture of 65 % E7 LC, 64.8% NOA-65 %, and 0.2% PI. Added various amounts (1×10^{-2} wt%, 5×10^{-2} wt. % and 10×10^{-2} wt. %) of f-CNTs dispersed in acetone was then added to above-mentioned mixture to obtain the desired f-CNT-PDLCs. To improve the degree of dopant dispersion level of f-CNTs in the PDLC mixture, the prepared mixtures were uniformly heated to an elevated temperature of 70 °C prior to ultrasonication for 3 h. Subsequently, acetone was evaporated by heating the sample mixture on a hot plate at 70 °C under stirring.

2.5. Device fabrication

The interdigitated electrode (IDE) substrates were cleaned by immersion in a detergent solution for 30 min. The substrates were then cleaned sequentially using deionized water, acetone, and isopropyl alcohol, followed by ultrasonication for 1 h to remove any remaining contaminants on the substrates. Prior to fabrication of the sensor device, the substrates were blustered with dry nitrogen gas to completely remove any remaining traces of solvent. The prepared sample mixtures were then drop-casted over the IDE substrates at 70 °C using a micropipette and spin-coated for 30 s at 3000 rpm. Subsequently, the sample substrates were phase-separated under UV light irradiation (40 mw/cm^2) for 10 min. The full details of the fabrication process of f-CNT-PDLC gas sensor was schematically illustrated in Fig. 2.

2.6. Gas detection response

Fig. 3 shows a schematic flow chart outlining the gas sensing setup used in the experiment. More specifically, to determine the gas sensing responses of the sensors, the fabricated PDLC and f-CNT-PDLC devices

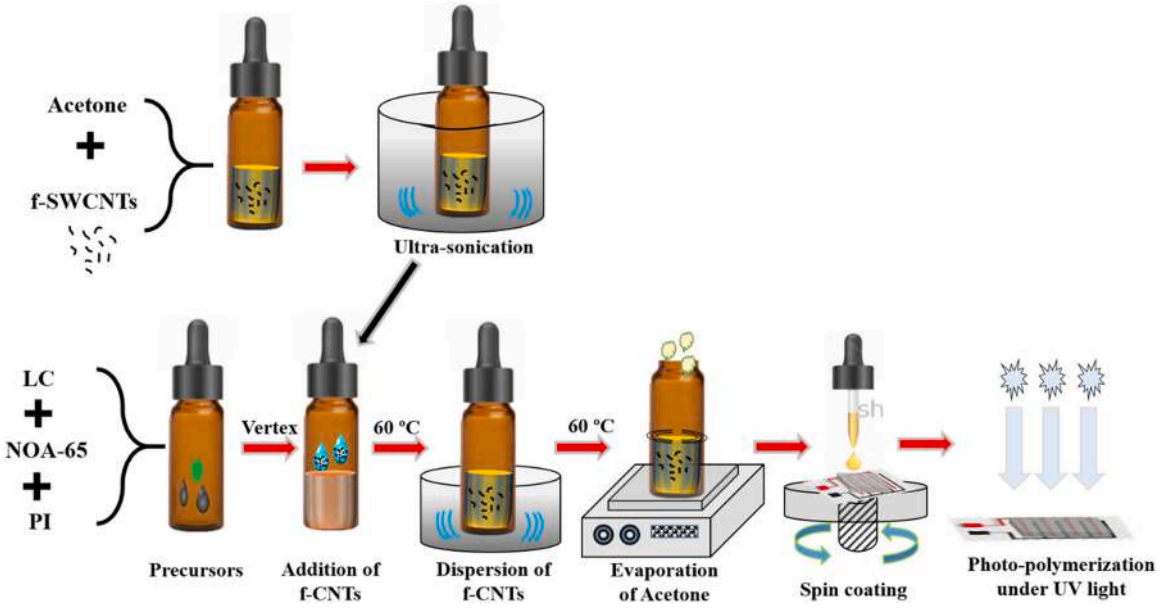

Fig. 2. Schematic representation of the f-CNT-doped PDCL composite preparation process.

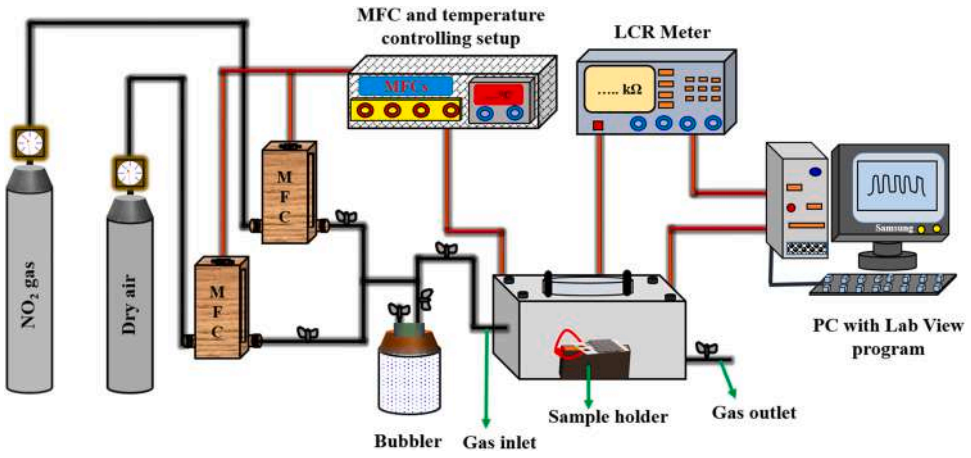

Fig. 3. Schematic flowchart illustrating the system setup employed for the gas sensing measurements.

were placed over the sample stage, and the metallic gas chamber was sealed to prevent leakage. The sample stage was maintained throughout the experiment at RT (27 °C) for the purpose of measuring the sensor response. Prior to carrying out the gas sensing measurements, the contaminated air molecules were evacuated from the gas chamber with the support of a rotary pump, and the pump was turned off during the tests. The sensor devices were subjected a square wave AC signal of 3 V at 1 kHz using a function generator, and the experiment was performed using the Labview program installed on a personal computer (PC). The humidity in the test chamber was developed by passing the dry through the water bubbler jar as shown in Fig. 3. The effective changes in the sensor responses were monitored by flowing the target gas and carrier gas through mass flow controllers (MFCs). The concentration of the analyte gas was determined using the following equation [37]:

$$C(ppm) = \left(\frac{f}{f+F}\right) \times C_{std}(ppm), \tag{5}$$

where f and F represent the analyte and carrier gas flow rates, respectively, and C_{std} (ppm) represents the analyte gas concentration in the gas cylinder. The C_{std} (ppm) values for all gases were 1000 ppm balanced with N_2, and the flow rates in the metallic gas chamber were maintained constant at 400 sccm throughout the experiment.

2.7. Characterization

Various characterization approaches were carried out to examine the PDLC and f-CNT-PDLC films. More specifically, to monitor the changes in the device resistances, the metallic gas chamber was connected externally to a network analyzer (HP, 8752C), a Keithley 2400 Graphical Series source measurement unit, and a function generator (Agilent 33521A). The wavelength-dependent absorption spectra were measured by UV–visible spectroscopy (SCINCO, S-3100) from the ultraviolet to the near-infrared region. In addition, Fourier-transform infrared (FT-IR) spectroscopy was employed to investigate the functional groups attached to the f-CNTs, while field-emission scanning electron microscopy (FE-SEM, S4700, Hitachi, Japan) was used to investigate the effect of the f-CNTs on the droplet morphology and the polymer matrix. For this purpose, the test devices were immersed in *n*-hexane for 48 h, and POM (ECLIPSE E600, Nikon, Japan) was used in conjunction with a CCD camera (DXM 1200, Nikon) to ensure the complete removal of the LC molecules from the polymer film. After careful investigation of the test cells, the test cells were separated using a sharp-knife blade, and the

substrate bearing the polymer film was placed in the oven at 80 °C for 1 h to remove all traces of *n*-hexane. The polymer surface was then covered with a thin platinum coating to prevent charge accumulation during characterization. Image-J software, a Java-based image processing program developed at the National Institutes of Health, was used to estimate the droplet size distribution.

3. Results and discussion

Following UV light treatment, the prepared PDLC and f-CNT-PDLC devices were subjected to various characterization techniques, which have been divided into two major sections for the purpose of this article. The first section discusses the surface morphological and spectroscopic characterization techniques, including FE-SEM, HR-TEM, UV–visible spectroscopy, and FT-IR spectroscopy, which were performed to determine the influence of the f-CNTs on the PDLCs. In the second part, the sensing responses of the devices under a NO_2 gas environment are described.

NO_2 gas sensing responses in terms of resistance for the sensor devices were determined with various weight-percentages of f-CNTs (1×10^{-2} wt.%, 5×10^{-2} wt.% and 10×10^{-2} wt.%) in the PDLC mixture. Fig. S2 depicts the sample resistance measured at RT when exposed to NO_2 gas at a concentration of 100 ppm for the controlled samples. This demonstrates that the sample loaded with 5.2×10^{-2} wt. % of f-CNTs has a high resistance in comparison to the other sensor devices.

3.1. Surface morphological studies

Fig. 4(a) shows the surface morphology of the as-prepared f-CNTs. More specifically, the HR-TEM image reveals that the f-CNTs are well dispersed, with the average length of each f-CNTs being ~250 ± 15 nm, and this can be attributed to the acidification process, which prevented significant aggregation. The surface morphology of the polymer network was also examined using FE-SEM to further determine the effect of the f-CNTs on the droplet morphology. Fig. 4(b–c) show the surface morphologies of the polymer networks and the relevant droplet size distributions along with the Gaussian fits (inset images) of the PDLC and f-CNT-PDLC samples, respectively. It should be noted here that the droplet size distributions of the samples were estimated with the help of Image-J software. The morphologies of the PDLC and f-CNT-PDLC films clearly demonstrate that the majority of droplets were distributed randomly throughout the polymer matrix, with average circular droplet diameters of 0.70 and 0.67 μm, respectively. Although the droplet size did not change significantly between the two films, the small degree of variation was attributed to the formation of a conductive network caused by the embedding of f-CNTs into the polymer matrix [29,39]. Importantly, the doped f-CNTs could not be observed on the polymer matrix, and so we assumed that they were blended into the polymer matrix owing to their small size [30]. The random distribution and encapsulation of f-CNTs in the polymer film not only results in the formation of a conductive network, but it also improves the physical properties of the hybrid sensing film [29,40–42].

3.2. Optical properties

3.2.1. UV–visible spectroscopy

The UV–vis absorption spectra of the various samples were then examined to determine the influence of the f-CNTs on the optical bandgap of the PDLC film. More specifically, Fig. 5 shows the optical absorption spectra of the prepared devices (i.e., the PDLC, and the f-CNT-PDLC devices) as a function of the wavelength in the 200–800 nm region. The sample mixtures were uniformly spin-coated onto quartz glass and were polymerized under the conditions described in the materials and methods section. The absorption spectra of PDLC and f-CNT-PDLC devices were recorded while passing the unpolarized incident light through the optical films. The absorption spectrum measured for pure PDLC device exhibited a maximum peak at 321.1 nm, while in the case of the f-CNT-PDLC device, the absorption peak was identified at 324.9 nm along with a small absorption peak corresponding to the f-CNTs at 284.2 nm. Besides, the spectrum recorded for the pure f-CNTs is shown in inset of Fig. 5(b), where the maximum absorption peak observed at 284.1 nm is in good agreement with previous studies [43]. When the f-CNTs are added to a PDLC mixture, the peak shifts towards higher wavelengths (i.e. red shifting), indicating a reduction in the band gap. In addition, the f-CNT-PDLC device shows increase in optical absorption as a result of this. The experimental evidences were obtained in the proposed device primarily as a result of the PDLC film being perturbed by the addition of f-CNTs. Furthermore, we observe that short-range elastic interactions between LC and f-CNTs, as well as interactions between polymer and f-CNTs that improve the dispersion level of f-CNTs up to a certain extent, resulting in improved electro-optical and optical properties of the host composite materials. Similar experimental results have been reported in the literature [21, 44].

3.2.2. FT-IR analysis

The surface active functional groups of the prepared samples were investigated using FT-IR spectroscopy in the wavenumber range of 400–4000 cm^{-1}. The full FT-IR spectrum recorded for the f-CNTs is given in Fig. 6(a), and the inset shows the broad absorption band observed at 3365 cm^{-1}, which can be attributed to the stretching vibration of the hydroxyl (OH) groups. In addition, the FT-IR spectra of the PDLC and f-CNT-PDLC devices presented in Fig. 6(b) clearly show absorption peaks at 2926, 2231, and 1710 cm^{-1}, which were associated with the C-H, C-N, and C-O bonds, and were ascribed to the characteristic structural modes of PDLC. Importantly, the observation of a peak corresponding to the nitrile group (C≡N) indicates the presence of LC

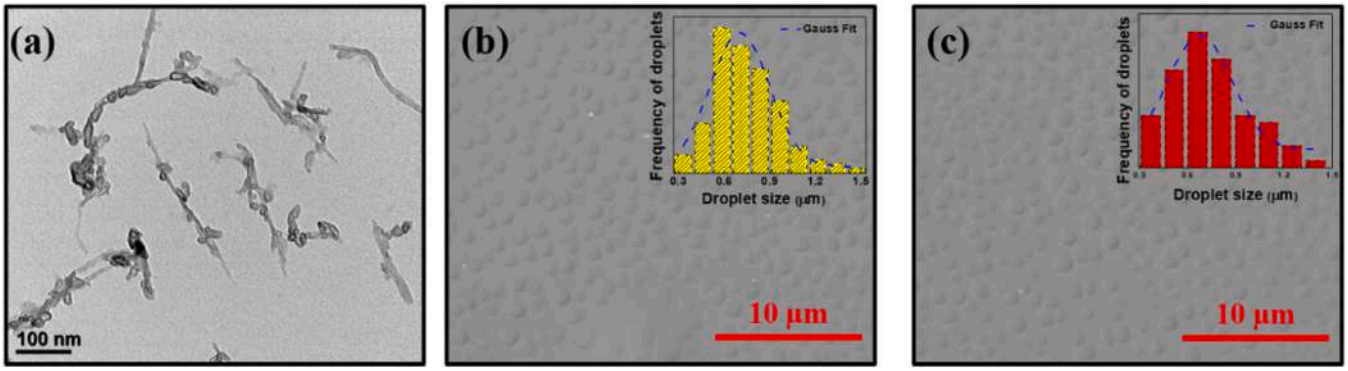

Fig. 4. (a) HR-TEM image of the dispersed f-CNTs, and FESEM images of the (b) PDLC and (c) f-CNT-PDLC polymer films (insets: droplet size distribution plots).

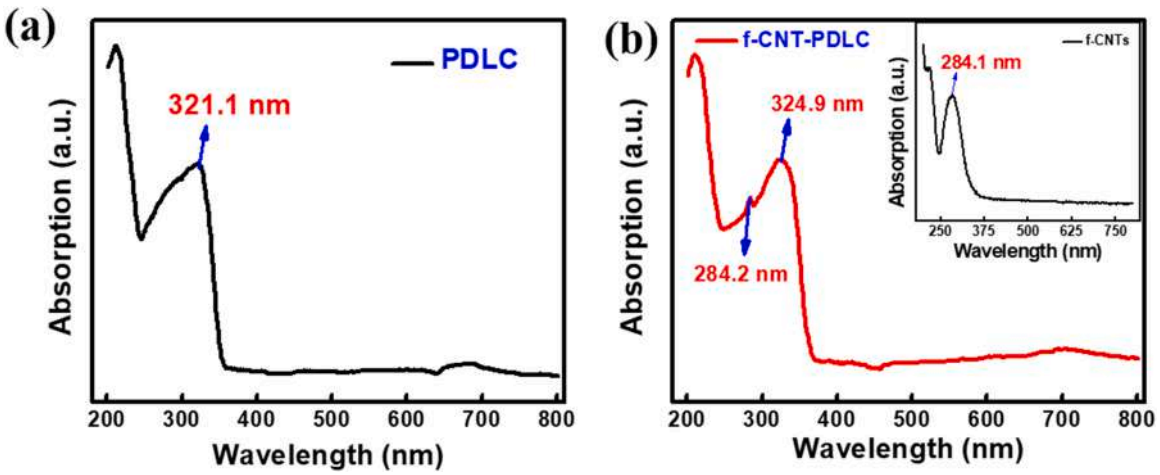

Fig. 5. Optical absorption spectrum of the (a) PDLC, and (b) f-CNT-PDLC sensor device. The inset shows image of f-CNT's absorption peak.

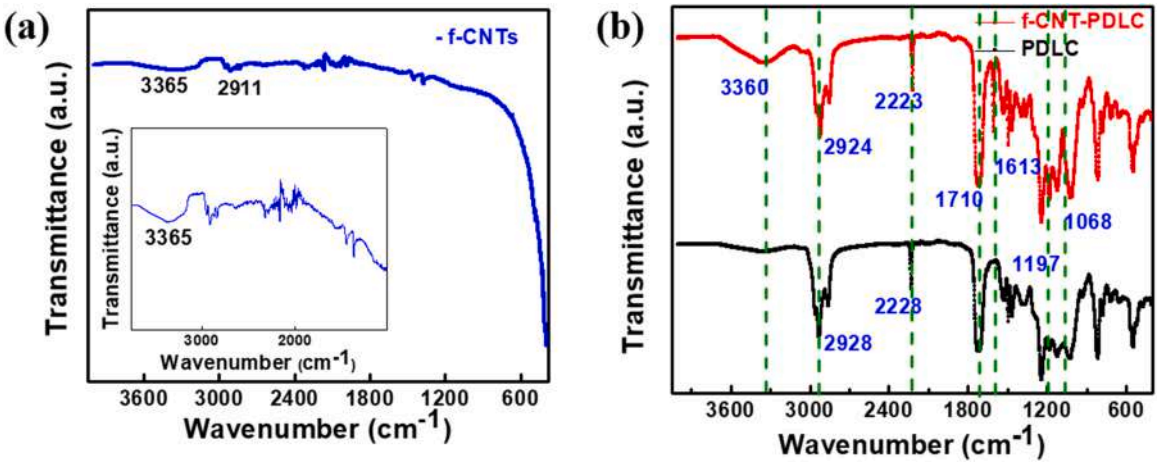

Fig. 6. FT-IR spectra of (a) the f-CNTs, and (b) the PDLC and f-CNT-PDLC devices.

molecules in the films [45]. Furthermore, the f-CNT-PDLC sample was found to exhibit some additional absorption peaks located at 3360, 1613, 1197, and 1068 cm^{-1}, which corresponded to the O-H, C═C, C-O, and C-O stretching vibrations, respectively, further confirming the presence of f-CNTs in the PDLC polymer film. It can also be observed that the characteristic peaks at 2924 and 1710 cm^{-1} were downshifted towards lower wavenumbers compared to the pristine PDLC sample. Moreover, the spectra show two additional pronounced peaks at 1613 and 3360 cm^{-1}, which were ascribed to the carboxyl (-COOH) and reactive hydroxyl (OH) functional groups, respectively, thereby confirming that the f-CNTs were successfully incorporated into the mixture [46]. It is noteworthy that upon comparison of the spectra recorded for the pristine PDLC and the f-CNT-PDLC composite system, the peaks of the latter shifted towards a lower wavenumber and the stretching bands were enhanced. This was considered to be due to electron delocalization in the composite system, which further aids in improving the interfacial charge transfer mechanism through short-range elastic interactions between the LCs and the f-CNTs within the droplets. In light of these experimental findings, we anticipated that the proposed f-CNT-PDLC device would exhibit significantly improved gas detection capabilities.

3.2.3. XPS analysis

The chemical compositions of the PDLC and f-CNT-PDLC films were investigated using X-ray photoelectron spectroscopy (XPS) over a wide range of binding energies between 0 and 1400 eV, and the experimental results are presented in Fig. 7. From survey spectra of Fig. 7(a), it can be seen that both the PDLC and f-CNT-PDLC devices exhibited three major peaks at 284.1 eV (C 1s), 399.4 eV (N 1s), and 532.0 eV (O 1s), in which C 1s and O 1s are dominant in f-CNT-PDLC, thereby confirming the carbon state in addition to OH-functionalization. In addition, the peak at 399.4 eV (N 1 s) exhibits a shift to lower binding energy between the PDLC and f-CNT-PDLC devices, which indicates the successful incorporation of f-CNTs into the LC droplets. Fig. 7(b–c) show the deconvolutions of the high-resolution C 1s and O 1s spectra of the f-CNT-PDLC device. More specifically, the C 1s spectrum presented in Fig. 7(b) shows a predominant peak at 284.6 eV corresponding to the abundant C═C sp^2 hybridized graphitic carbon species; the peaks at 286.2 eV (C-OH) and 288.8 eV (C═O) correspond to the hydroxyl and carbonyl groups, respectively. As indicated in Fig. 7(a), the oxygen component increases in the case of the f-CNT-PDLC sensor, wherein the core-level spectrum of O 1s displayed two major peaks at 531.9 eV (C-OH) and 533.4 eV (O-C═O), indicating that all oxygen atoms are bonded to the f-CNTs in the form of carbonyl and hydroxyl groups (Fig. 7(c)).

3.2.4. Polarized optical microscopy

The phase behavior of the proposed f-CNT-PDLC sensor device was examined by POM following exposure to UV light. Fig. 8 shows the POM and optical microscopy (OM) images of the f-CNT-PDLC sensor captured with crossed and single polarizers. More specifically, the POM image presented in Fig. 8(a) exhibits macroscopic scattering of the incident light, which is caused by the random orientation of the LC director with respect to the adjacent LC and any sub-wavelength-sized LC droplets. In

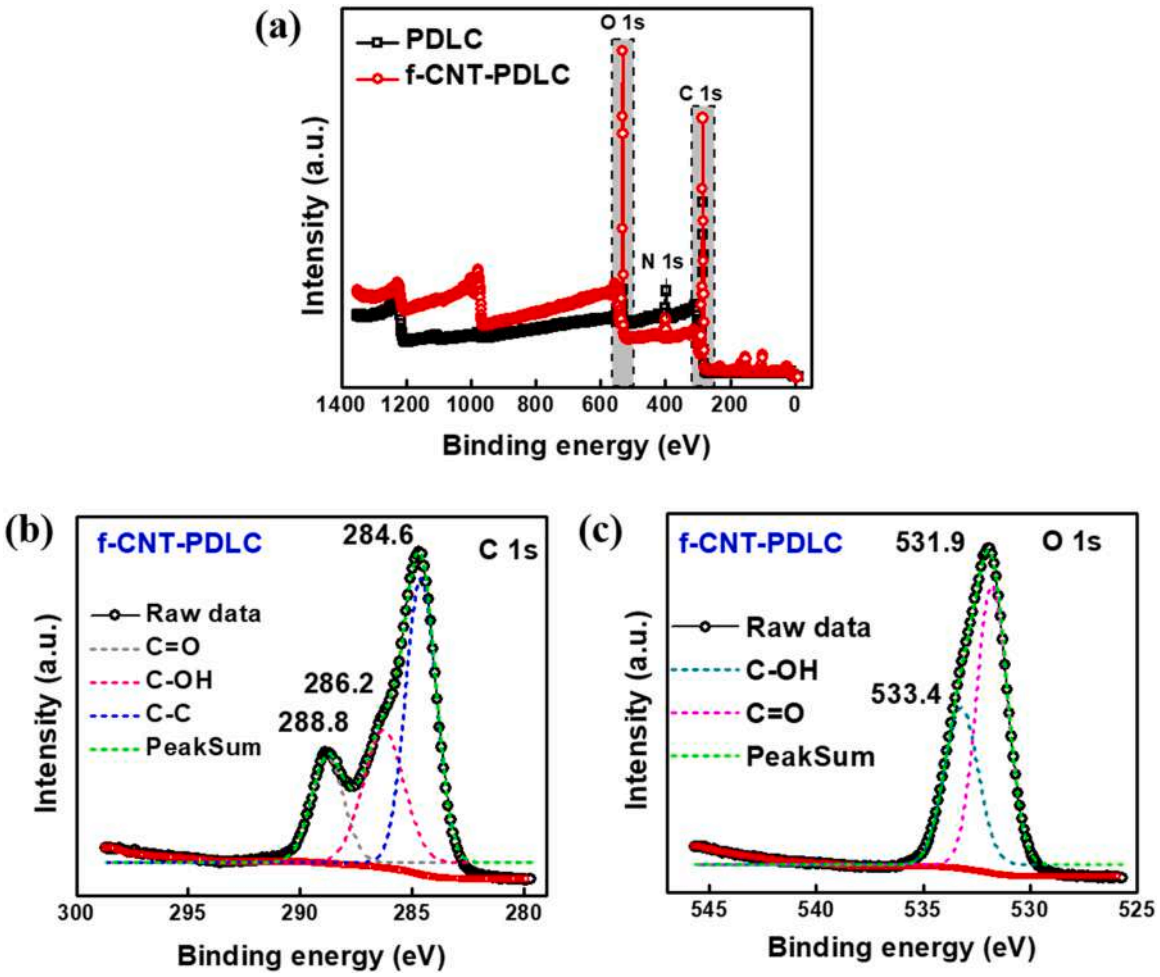

Fig. 7. (a) XPS survey spectra for the PDLC and f-CNT-PDLC devices, (b, c) Deconvoluted XPS core level high-resolution spectra of C 1s and O 1s for the f-CNT-PDLC device.

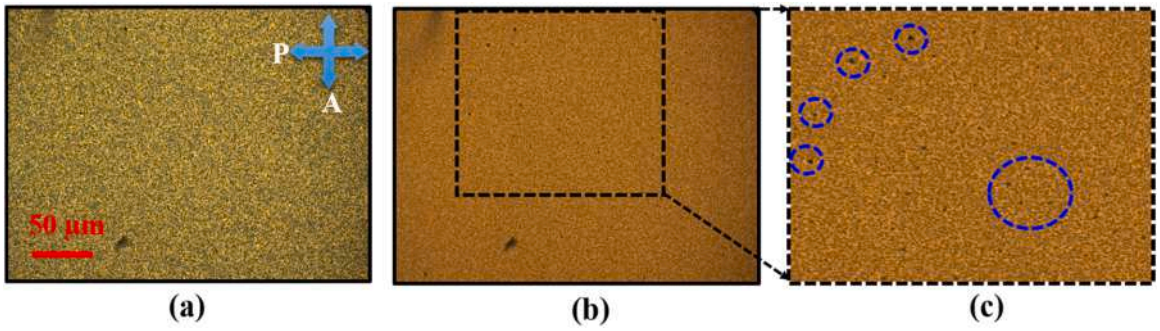

Fig. 8. (a) Polarized optical microscopy (POM) image and (b) Optical microscopy (OM) image of the f-CNT-PDLC sensor film. (c) Magnified OM image of the undispersed f-CNTs in the f-CNT-PDLC sensor (blue circles).

general, the Rayleigh-Gans scattering approximation can be used to explain the light scattering of a device, which is defined as the average scattering cross-section (σ_s) being inversely proportional to the fourth power of the wavelength of incident light (λ^4) [47]. In addition, the OM image of the sensor device shown in Fig. 8(b) indicates that the f-CNTs appear to be uniformly dispersed within the polymer matrix, although a few agglomerates were observed in the matrix, as indicated in blue Fig. 8 (c). Based on the observations of f-CNT agglomerates in the OM images, we can anticipate that these consisted of stronger van der Waals interactions, and that the monomer was highly viscose.

3.2.5. Gas sensing response

We prepared two different samples (PDLC and f-CNT-PDLC) to understand the influence of doped f-CNTs on PDLC devices in terms of the direct interaction with NO_2 gas molecules. During the experiment, the target NO_2 gas was mixed with the carrier gas and passed through the gas chamber at a concentration of 100 ppm. Fig. 9 depicts the NO_2 gas sensing properties in terms of the sample resistance of the PDLC and f-CNT-PDLC devices with the gas concentration of 100 ppm at RT (27 °C). It was noted that the resistance of each device increased with the concentration of the gas until it reached a saturation level, after which it returned to its original base resistance when the NO_2 gas was turned off.

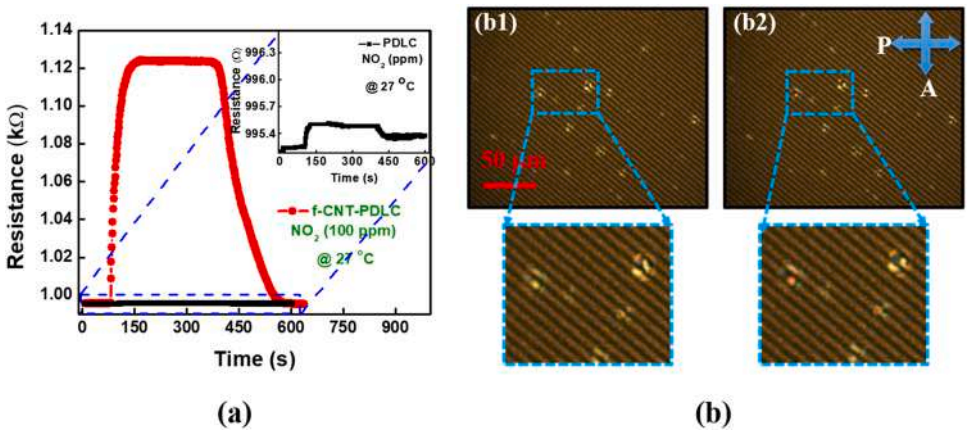

Fig. 9. (a) Resistance measured for the PDLC and f-CNT-PDLC sensors tested with a NO_2 gas concentration of 100 ppm. (b) At $E < E_{th}$, POM images of the f-CNT-PDLC sensor under crossed polarizers, (b1) LC droplet in the absence of NO_2, and (b2) Restructured LC droplet in the presence of NO_2. The magnified images show the orientations of the corresponding LC droplets.

When the same amount of NO_2 gas is passed through both the f-CNT-PDLC and the pure PDLC sensors, it was discovered that the sensor resistance of the f-CNT-PDLC was significantly higher. Besides the resistance of the f-CNT-PDLC device returned to the ground level in comparison to PDLC sensor as the switching the target gas flow back to the carrier gas. The high resistance exhibited by the f-CNT-PDLC device demonstrates that the presence of the f-CNT dopant is essential to achieving recognition of the target gas molecules; for this NO_2 gas concentration of 100 ppm, the f-CNT-PDLC sensor device yields a significant gas sensing response of about ~12.9% which was much higher than the pristine PDLC device to 100 ppm of NO_2 gas at RT. In the present study, the transient sensing responses were estimated using Eq. (4).

Subsequently, the orientation of the LC droplets encapsulated in the polymer matrix was investigated by observing the molecular changes taking place when the sensor device was exposed to the NO_2 target gas. The POM images recorded for the f-CNT-PDLC in the presence and absence of NO_2 gas are shown in Fig. 9(b), wherein it can be seen that the molecular orientation of the LC droplet remained stable in the absence of NO_2 gas (enlarged Fig. 9(b1)) since the LC molecules within the polymer matrix were partially influenced as a result of the electric fields ($E < E_{th}$) and the predetermined orientation of the f-CNTs. In contrast, in the presence of NO_2, the droplet orientation changed (enlarged Fig. 9(b2)) despite the fact that the NO_2 gas did not significantly influence the bulk property of the LC orientation due to the limited number of NO_2 molecules introduced into the system. The observed sensing capabilities of the f-CNT-PDLC device for NO_2 gas were therefore primarily attributed to the trapping of gas molecules on the surfaces of the f-CNTs through the oxidation of NO_2. We therefore anticipate that the absorption of gas molecules causes a change in the orientation phases of the LCs and the f-CNTs within the droplet rather than altering the orientation of all LC molecules throughout the device.

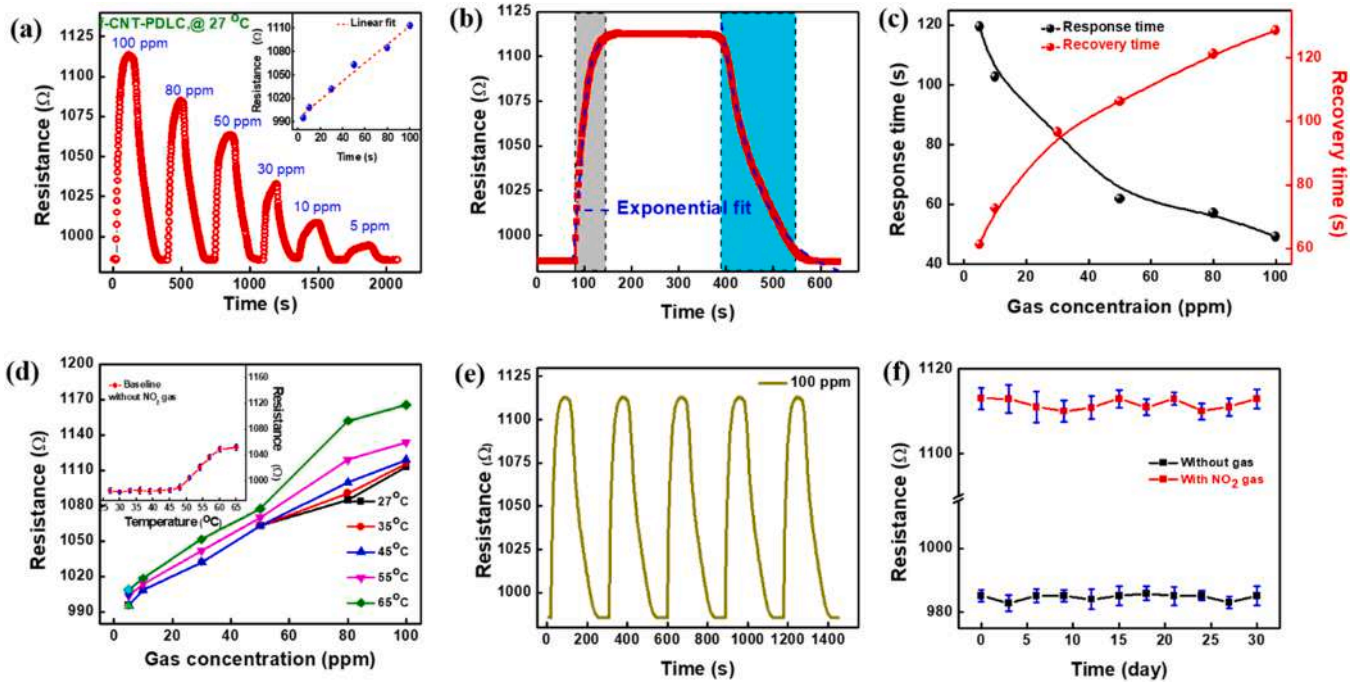

Fig. 10. (a,c) Transient responses in addition to response and recovery time curves for the f-CNT-PDLC device at various NO_2 gas concentrations. (b) Bi-exponential fittings for the response and recovery times measured at 100 ppm NO_2, (d) Temperature dependent sensing properties ranging from 27 °C to 65 °C with and without NO_2 gas, (e) Cyclic stability towards 100 ppm of NO_2 gas at 27 °C, and (f) Long-term stability toward 100 ppm NO_2 gas over 30 days at 27 °C.

The dynamic transient gas response and switching (response/recovery) time of the proposed f-CNT-PDLC device as a function of the NO_2 gas concentration were then investigated (Fig. 10). For the purpose of this experiment, the target NO_2 gas was mixed with the carrier gas at various concentrations (5–100 ppm) and passed through the gas chamber because the responses of the sensor rely on various concentrations of target NO_2 gas molecules. Fig. 10(a) shows the response and recovery curves of the f-CNT-PDLC sensor when exposed to various concentrations of NO_2 gas measured at RT. From Fig. 10(a) it can be obvious that with decreasing the NO_2 gas molecules concentration from 100 to 5 ppm level the response decreases. In addition, the inset image of Fig. 10(a) shows that the distinguished relative resistance of the f-CNT-PDLC sensor measured over this range of gas concentrations increased linearly with an increasing NO_2 gas concentration. The linear fittings executed of the sensor device exhibited almost linear response to NO_2 gas molecule concentration with the same correlation coefficient of $R^2 = 0.983$. In addition, we also estimate the detection limit (DL) of the proposed f-CNT-PDLC sensor device using the following equations,

$$DL = 3\left(\frac{RMS_{noise}}{slope}\right), \tag{6}$$

$$RMS_{noise} = \sqrt{\left(R_i - R_f\right)^2 \Big/ N}, \tag{7}$$

where RMS is the root mean square noise that is the base line noise level of the sensor response under air estimated from the fifth polynomial fit as shown in Fig. S3(a) and R_i and R_f are the experimental and fitting points that are extracted from polynomial fit and N is the total number of base-line points. The slope was taken from the linear fitting shown in Fig. S3(b). The estimated theoretical DL of the proposed f-CNT-PDLC sensor device is 244 ppb.

The estimated dynamic switching response and recovery times obtained by exponential fitting of the NO_2 gas concentration at 100 ppm are shown in Fig. 10(b). The response and recovery times are defined here as the time required to change the response from 10 % to 90 % in the presence of NO_2, and from 90 % to 10 % after stopping the NO_2 flow. As shown in Fig. 10(c), the measured experimental parameters of the response time gradually decreased with an increasing gas concentration, whereas the recovery time exhibited the opposite dependence on the gas concentration. As expected, the response times were shorter at higher gas concentrations because a large number of NO_2 gas molecules were available to react with f-CNTs at a given time, thereby changing the direction of LC molecules from a stable to an isotropic state. In contrast, the absorbed gas molecules required longer times to desorb from the f-CNT surface due to their penetration on the sample surface. As a result, the recovery times required for reorientation of the LC molecules from the isotropic to the preferred direction were slow. The orientational phases change of the LC droplet during the absorption or desorption of NO_2 gas molecules were ascribed to the presence of induced short-range elastic interactions between the LCs and f-CNTs within the droplet, as shown schematically in Fig. 1. Similar observations have also been reported for CNTs, in which strong molecular reorientations were observed as a result of external stimuli, such as an applied electric field or a change in the target gas molecule concentration [15,20,29,31], thereby supporting that the external stimulus of introduction NO_2 gas causes the observed orientational phase changes in the LC droplets in the presence of NO_2-f-CNT interactions.

In addition, we investigate the effect of temperature on NO_2 gas sensing performance of f-CNT-PDLC sensor device at various temperature ranging from 27 °C (RT) to 65 °C by varying the target NO_2 gas (10–100 ppm) in order to determine the obtained sensing effect is not caused by temperature. Fig. 10(d) shows that the resistance of f-CNT-PDLC sensor device increases with temperature in the presence of NO_2 gas, on the other hand, in the absence of NO_2 gas, the resistance is nearly consistent up to 48 °C and then increases with increasing the temperature up to 65 °C as shown in inset of Fig. 10(d). The increase in resistance noticed in the absence of NO_2 gas can be attributed to two possible reasons: i) thermal energy and ii) re-orientation of LC droplets from their preferred state to isotropic state. The resistance of f-CNT-PDLC sensor increased with temperature with a maximum resistance of 4.7 % to 100 ppm of NO_2 at 65 °C compared to resistance at RT (27 °C). The increased resistance of the f-CNT-PDLC sensor at higher temperature is attributed to high thermal energy that offers a large number of absorption sites on the f-CNTs, attracting a large number of NO_2 gas molecules at higher ppm concentration levels.

Due to the importance of the cycling stability of a gas sensing device in terms of its reproducibility for real-time device applications, the cycling stability of the proposed f-CNT-PDLC sensor in response to the NO_2 gas concentration was investigated (Fig. 10(e)). As can be seen from this figure, the proposed f-CNT-PDLC device exhibited a highly stable and reproducible gas sensing performance, wherein the transient response as well as the response and recovery times toward NO_2 gas remain constant until the end of each repeated cycle. Furthermore, the stable NO_2 gas sensing responses for the five consecutive repeatable cycles were estimated, and it demonstrated a stable response of about ~12.9 % for 100 ppm levels at RT without any interruptions, indicating that the f-CNT-PDLC sensor has good stability towards NO_2 gas. Fig. 10 (f) shows the long-term stability of the f-CNT-PDLC sensor performed at 27 °C with 100 ppm of NO_2 gas for 30 days. This manifests that the measured resistance of the device remained relatively consistent over the one-month testing period with no evidence of fluctuations were identified with and without NO_2 gas.

Furthermore, the relative humidity (RH) and selectivity testing was performed because these are an additional important factors that can affect the sensing performances of the practical device applications. Fig. 11(a) shows the effect of RH on the response of f-CNT-PDLC investigated at RT under various RH conditions ranging from 0 % to 80 % in the absence and presence of NO_2 gas (100 ppm). When the RH levels increased from 0 % to 80 %, the resistance of f-CNT-PDLC device remained consistent in the absence of target NO_2 gas, whereas it gradually decreased in the presence of NO_2 gas (100 ppm). The decrease in sensing response is primarily ascribed to the blocking of active sites on the sensor device by the water (O_2) molecules interface between NO_2 gas, which could restrict and minimize O_2 molecule absorption, besides, it increases as RH levels increase [48,49]. Moreover, the selectivity is examined to the proposed f-CNT-PDLC sensor device to examine whether it responds to additional harmful gases, such as NO_2, H_2S, CO, H_2 and NH_3. Such selectivity tests in the context of potential interferants is also of particular importance when designing devices for sensing applications. Thus, Fig. 11(b) shows the experimental results obtained during the selectivity test with a fixed gas concentration of 100 ppm for each gas at RT. It manifests that the proposed f-CNT-PDLC sensor exhibited significantly higher sensing responses towards interferant H_2S, CO, H_2 and NH_3 gases, respectively. Based on this experimental evidence, we clearly anticipate that the proposed f-CNT-PDLC sensor would demonstrate a superior NO_2 gas selectivity and can be considered a promising candidate for development in the context of environmental and biomedical device applications.

4. Conclusion

We successfully demonstrated the development of a versatile resistive-type functionalized-carbon nanotube-doped polymer dispersed liquid crystal (f-CNT-PDLC) gas sensor. The optical and chemical compositional properties of the prepared PDLC and f-CNT-PDLC sensors were studied using a range of analytical techniques to determine the influence of f-CNT doping on the properties of the PDLCs. It was found that due to the presence of these conductive f-CNTs, the proposed f-CNT-PDLC device exhibited an enhanced optical bandgap and an established conductive pathway within its polymer network. Moreover, the f-CNT absorption sites and the presence of hydroxyl functional groups were

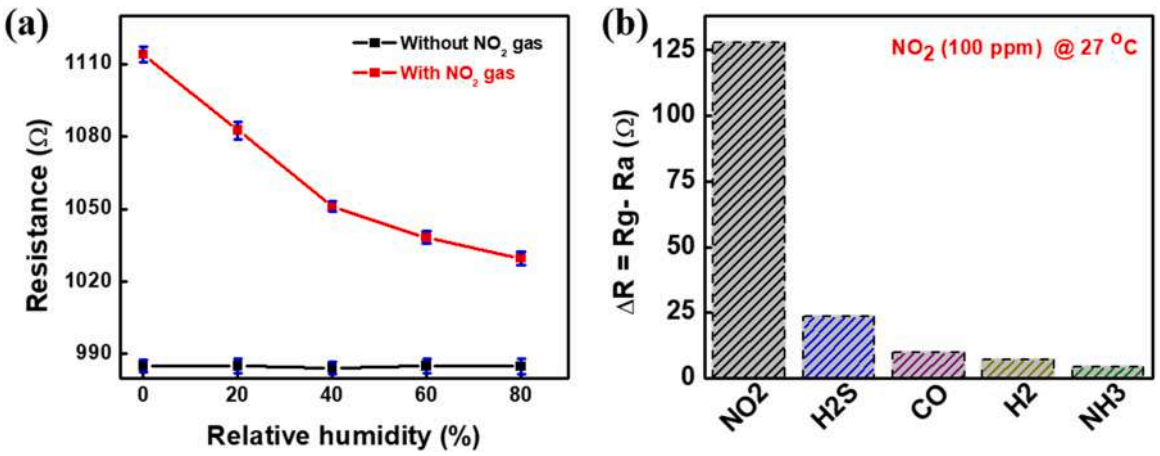

Fig. 11. (a) Relative humidity (RH) ranging from 0% to 80% with and without 100 ppm of NO_2 gas at RT (27 °C), and (b) Selectivity test towards various interferant gases NO_2, H_2S, CO, H_2 and NH_3 of 100 ppm at RT (27 °C).

demonstrated to play a pivotal role in the detection of NO_2 gases by changing the orientational transition ordering of the induced short-range elastic interactions within the droplets. In addition, the f-CNT-PDLC device exhibited excellent NO_2 gas sensing properties at RT, with a response of 12.9% at a NO_2 gas concentration of 100 ppm, and a good selectivity against other gases, such as H_2S, CO, H_2, and NH_3. Furthermore, the sensor device was tested under various RH conditions and the obtained results revealed that the sensing responses were decreased as the RH levels increased. Moreover, the transient response was found to be linearly related to the gas concentration and exhibited a good cyclic repeatability for up to five measurement cycles. Based on its superior performance, we believe that the proposed f-CNT-PDLC sensor can make a significant contribution towards the detection of diverse analytes and the application of LCs to next-generation flexible/wearable photonic devices.

CRediT authorship contribution statement

Srinivas Pagidi: Conceptualization, Methodology, Investigation, Data curation, Validation, Writing - original draft. **Kedhareswara Sairam Pasupuleti:** Formal analysis, Visualization, Writing - review & editing. **Maddaka Reddeppa:** Formal analysis, Visualization, Writing - review & editing. **Soyeon Ahn:** Formal analysis. **Youngseo Kim:** Formal analysis. **Jong-Hyun Kim:** Formal analysis. **Moon-Deock Kim:** Formal analysis. **Seung Hee Lee:** Formal analysis, Conceptualization, Visualization, Writing - review & editing, Supervision. **Min Yong Jeon:** Conceptualization, Visualization, Validation, Writing - review & editing, Supervision.

Declaration of Competing Interest

The authors declare that they have no known competing financial interests or personal relationships that could have appeared to influence the work reported in this paper.

Acknowledgments

This research was supported by Basic Science Research Program through the National Research Foundation of Korea (NRF) funded by the Ministry of Science, ICT and Future Planning (NRF-2019R1A2C1084933, NRF-2019R1A5A8080326 NRF-2020R1A6A1A03047771) and was supported by a Korea Institute for Advancement of Technology (KIAT) grant funded by the Korea Government (MOTIE) (P0008458, The Competency Development Program for Industry Specialist).

Appendix A. Supporting information

Supplementary data associated with this article can be found in the online version at doi:10.1016/j.snb.2022.132482.

References

[1] A. Dey, Semiconductor metal oxide gas sensors: a review, Mater. Sci. Eng. B 229 (2018) 206–217.
[2] S.J. Park, C.S. Park, H. Yoon, Chemo-electrical gas sensors based on conducting polymer hybrids, Polymers 9 (2017) 155.
[3] A. Mirzaei, S. Leonardi, G. Neri, Detection of hazardous volatile organic compounds (VOCs) by metal oxide nanostructures-based gas sensors: a review, Ceram. Int. 42 (2016) 15119–15141.
[4] M. Chen, Z. Liu, Y. Guan, Y. Chen, W. Liu, Y. Liu, Zeolitic imidazolate frameworks-derived hollow Co/N-doped CNTs as oxidase-mimic for colorimetric-fluorescence immunoassay of ochratoxin A, Sens. Actuators B Chem. 359 (2022), 131609.
[5] J. Liu, L. Zhang, J. Fan, B. Zhu, J. Yu, Triethylamine gas sensor based on Pt-functionalized hierarchical ZnO microspheres, Sens. Actuators B Chem. 331 (2021), 129425.
[6] D. Dunmur, T. Sluckin, Soap, Science, and Flat-screen TVs: a History of Liquid Crystals, Oxford University Press, 2014.
[7] M. Bremer, P. Kirsch, M. Klasen-Memmer, K. Tarumi, The TV in your pocket: development of liquid-crystal materials for the new millennium, Angew. Chem. Int. Ed. 52 (2013) 8880–8896.
[8] S.N. Fernandes, P.L. Almeida, N. Monge, L.E. Aguirre, D. Reis, C.L. de Oliveira, et al., Mind the microgap in iridescent cellulose nanocrystal films, Adv. Mater. 29 (2017), 1603560.
[9] C.-M. Chang, Y.-H. Lin, A.K. Srivastava, V.G. Chigrinov, An optical system via liquid crystal photonic devices for photobiomodulation, Sci. Rep. 8 (2018) 1–10.
[10] R.J. Carlton, J.T. Hunter, D.S. Miller, R. Abbasi, P.C. Mushenheim, L.N. Tan, et al., Chemical and biological sensing using liquid crystals, Liq. Cryst. Rev. 1 (2013) 29–51.
[11] X. Ding, K.-L. Yang, Liquid crystal based optical sensor for detection of vaporous butylamine in air, Sens. Actuators B Chem. 173 (2012) 607–613.
[12] C.G. Reyes, A. Sharma, J.P. Lagerwall, Non-electronic gas sensors from electrospun mats of liquid crystal core fibres for detecting volatile organic compounds at room temperature, Liq. Cryst. 43 (2016) 1986–2001.
[13] M. Sargazi, M.R. Linford, M. Kaykhaii, Liquid crystals in analytical chemistry: a review, Crit. Rev. Anal. Chem. 49 (2019) 243–255.
[14] J. Wang, A. Jákli, J.L. West, Liquid crystal/polymer fiber mats as sensitive chemical sensors, J. Mol. Liq. 267 (2018) 490–495.
[15] Y.-T. Lai, J.-C. Kuo, Y.-J. Yang, A novel gas sensor using polymer-dispersed liquid crystal doped with carbon nanotubes, Sens. Actuators B Chem. 215 (2014) 83–88.
[16] P.K. Chan, A.D. Rey, Polymerization-induced phase separation. 1. Droplet size selection mechanism, Macromolecules 29 (1996) 8934–8941.
[17] C.-M. Chang, Y.-H. Lin, V. Reshetnyak, C.H. Park, R. Manda, S.H. Lee, Origins of Kerr phase and orientational phase in polymer-dispersed liquid crystals, Opt. Express 25 (2017) 19807–19821.
[18] S. Bronnikov, S. Kostromin, V. Zuev, Polymer-dispersed liquid crystals: progress in preparation, investigation, and application, J. Macromol. Sci. B 52 (2013) 1718–1735.
[19] F. Roussel, C. Canlet, B.M. Fung, Morphology and orientational order of nematic liquid crystal droplets confined in a polymer matrix, Phy. Rev. E 65 (2002), 021701.
[20] Y.-T. Lai, J.-C. Kuo, Y.-J. Yang, Polymer-dispersed liquid crystal doped with carbon nanotubes for dimethyl methylphosphonate vapor-sensing application, Appl. Phys. Lett. (2013), 191912.

[21] Y. Liu, J. Zheng, Z. Jiang, Q. Zhu, Q. Chen, S. Zhuang, Optical and dielectric analysis of ZnO nanorods doped polymer dispersed liquid crystal and ethanol gas sensing investigation, Liq. Cryst. 47 (2020) 2247–2256.
[22] Y. Liu, J. Zheng, Q. Zhu, T. Shen, Q. Chen, Impedance spectroscopy investigation of ZnO nanorod doped polymer-dispersed liquid crystal for ethanol gas sensing, ECS J. Solid State Sci. Technol. 9 (2020), 063007.
[23] M. Spengler, L. Pschyklenk, J. Niemeyer, P. Kaul, M. Giese, Photonic NO2 gas sensing with binaphthyl-based dopants, Adv. Opt. Mater. 9 (2021), 2001828.
[24] A. Sen, K.A. Kupcho, B.A. Grinwald, H.J. VanTreeck, B.R. Acharya, Liquid crystal-based sensors for selective and quantitative detection of nitrogen dioxide, Sens. Actuators B Chem. 178 (2013) 222–227.
[25] J. Suehiro, G. Zhou, M. Hara, Fabrication of a carbon nanotube-based gas sensor using dielectrophoresis and its application for ammonia detection by impedance spectroscopy, J. Phys. D: Appl. Phys. 36 (2003) L109.
[26] T. Helbling, R. Pohle, L. Durrer, C. Stampfer, C. Roman, A. Jungen, et al., Sensing NO2 with individual suspended single-walled carbon nanotubes, Sens. Actuators B Chem. 132 (2008) 491–497.
[27] C. Cantalini, L. Valentini, I. Armentano, L. Lozzi, J. Kenny, S. Santucci, Sensitivity to NO2 and cross-sensitivity analysis to NH3, ethanol and humidity of carbon nanotubes thin film prepared by PECVD, Sens. Actuators B Chem. 95 (2003) 195–202.
[28] K.H. An, S.Y. Jeong, H.R. Hwang, Y.H. Lee, Enhanced sensitivity of a gas sensor incorporating single-walled carbon nanotube–polypyrrole nanocomposites, Adv. Mater. 16 (2004) 1005–1009.
[29] S. Pagidi, R. Manda, S.S. Bhattacharyya, K.J. Cho, T.H. Kim, Y.J. Lim, et al., Superior electro-optics of nano-phase encapsulated liquid crystals utilizing functionalized carbon nanotubes, Compos. B. Eng. 164 (2019) 675–682.
[30] W. Tie, S.S. Bhattacharyya, Y. Zhang, Z. Zheng, T.H. Lee, S.W. Lee, et al., Field-induced stretching and dynamic reorientation of functionalized multiwalled carbon nanotube aggregates in nematic liquid crystals, Carbon 96 (2016) 548–556.
[31] S.Y. Jeon, S.H. Shin, S.J. Jeong, S.H. Lee, S.H. Jeong, Y.H. Lee, et al., Effects of carbon nanotubes on electro-optical characteristics of liquid crystal cell driven by in-plane field, Appl. Phys. Lett. 90 (2007), 121901.
[32] P. Kumar, V. Sharma, C. Jaggi, P. Malik, K.K. Raina, Orientational control of liquid crystal molecules via carbon nanotubes and dichroic dye in polymer dispersed liquid crystal, Liq. Cryst. 44 (2017) 843–853.
[33] I. Dierking, G. Scalia, P. Morales, D. LeClere, Aligning and reorienting carbon nanotubes with nematic liquid crystals, Adv. Mater. 16 (2004) 865–869.
[34] C. Zamora-Ledezma, C. Blanc, N. Puech, M. Maugey, C. Zakri, E. Anglaret, et al., Conductivity anisotropy of assembled and oriented carbon nanotubes, Phys. Rev. E. 84 (2011), 062701.
[35] H. Chang, J.D. Lee, S.M. Lee, Y.H. Lee, Appl. Phys. Lett. 79 (2001) 3863.
[36] L. Valentini, I. Armentano, J. Kenny, C. Cantalini, L. Lozzi, S. Santucci, Sensors for sub-ppm NO 2 gas detection based on carbon nanotube thin films, Appl. Phys. Lett. 82 (2003) 961–963.
[37] M. Reddeppa, T.K.P. Nguyen, B.-G. Park, S.-G. Kim, M.-D. Kim, Low operating temperature NO gas sensors based hydrogen peroxide treated GaN nanorods, Phys. E: Low. -Dimens. Syst. Nanostruct. 116 (2020), 113725.
[38] P.-G. Su, S. Lin-Kuo, H 2-gas sensing and discriminating actions of a single-yarn sensor based on a Pd/GO multilayered thin film using FFT, Anal. Methods 12 (2020) 3537–3544.
[39] S. Pagidi, R. Manda, H.S. Shin, J. Lee, Y.J. Lim, M. Kim, et al., Enhanced electro-optic characteristics of polymer-dispersed nano-sized liquid crystal droplets utilizing PEDOT: PSS, Polym. Compos., J. Mol. Liq. 322 (2021), 114959.
[40] N. Lebovka, T. Dadakova, L. Lysetskiy, O. Melezhyk, G. Puchkovska, T. Gavrilko, et al., Phase transitions, intermolecular interactions and electrical conductivity behavior in carbon multiwalled nanotubes/nematic liquid crystal composites, J. Mol. Struct. 887 (2008) 135–143.
[41] H.-C. Jeong, E.M. Kim, G.-S. Heo, J.H. Lee, J.H. Won, D.H. Kim, et al., Effect of the physicochemical modification on bismuth-doped zinc oxide in the anisotropic orientation of liquid crystal molecules, ECS J. Solid State Sci. Technol. 9 (2020), 043001.
[42] I. Studenyak, P. Kopčanský, M. Timko, Z. Mitroova, O. Kovalchuk, Effects of non-additive conductivity variation for a nematic liquid crystal caused by magnetite and carbon nanotubes at various scales, Liq. Cryst. 44 (2017) 1709–1716.
[43] R. Verma, M. Mishra, R. Dhar, R. Dabrowski, Single walled carbon nanotubes persuaded optimization of the display parameters of a room temperature liquid crystal 4-pentyl-4′ cyanobiphenyl, J. Mol. Liq. 221 (2016) 190–196.
[44] G. Pathak, S. Pandey, R. Katiyar, A. Srivastava, R. Dabrowski, K. Garbat, et al., Analysis of photoluminescence, UV absorbance, optical band gap and threshold voltage of TiO2 nanoparticles dispersed in high birefringence nematic liquid crystal towards its application in display and photovoltaic devices, J. Lumin. 192 (2017) 33–39.
[45] M. Kim, K.J. Park, S. Seok, J.M. Ok, H.-T. Jung, J. Choe, et al., Fabrication of microcapsules for dye-doped polymer-dispersed liquid crystal-based smart windows, ACS Appl. Mater. Interfaces 7 (2015) 17904–17909.
[46] K.S. Pasupuleti, M. Reddeppa, D.-J. Nam, N.-H. Bak, K.R. Peta, H.D. Cho, et al., Boosting of NO2 gas sensing performances using GO-PEDOT: PSS nanocomposite chemical interface coated on langasite-based surface acoustic wave sensor, Sens. Actuators B Chem. (2021), 130267.
[47] G.P. Montgomery Jr, J.L. West, W. Tamura-Lis, Light scattering from polymer-dispersed liquid crystal films: droplet size effects, J. Appl. Phys. 69 (1991) 1605–1612.
[48] M. Reddeppa, N.T. KimPhung, G. Murali, K.S. Pasupuleti, B.-G. Park, I. In, et al., Interaction activated interfacial charge transfer in 2D g-C3N4/GaN nanorods heterostructure for self-powered UV photodetector and room temperature NO2 gas sensor at ppb level, Sens. Actuators B Chem. 329 (2021), 129175.
[49] N.D. Chinh, C. Kim, D. Kim, UV-light-activated H2S gas sensing by a TiO2 nanoparticulate thin film at room temperature, J. Alloy. Compd. 778 (2019) 247–255.

Dr. Srinivas Pagidi, Dr. Srinivas Pagidi received his M.Sc. in Physics (2009) and M.Tech. Materials Engineering (2015) degrees from University of Hyderabad, Hyderabad, India, and the Ph.D. from the Department of BIN Convergence Technology at Jeonbuk National University in Jeonju, Republic of Korea, in 2020 under the supervision of Prof. Seung Hee Lee's research group. He is currently working a Postdoctoral researcher in Prof. Min Yong Jeon's research group at Department of Physics, Chungnam National University, Daejeon, Republic of Korea. His current research interest is focused on development of high-performance nano/micro-sized liquid crystal droplets embedded in a polymer matrix for various device applications including displays, switchable 2D/3D micro-lenticular lenses, diffraction gratings and gas sensors.

Kedhareswara Sairam Pasupuleti received his Master's degree in Physics with a specialization of Thin films and Vacuum technology from Sri Venkateswara University, Tirupati, India, in 2018. He is a Ph.D. student in the department of Physics, Chungnam National University, Republic of Korea. He is currently working on III–V nitride semiconductors and SAW gas sensors.

Dr. Maddaka Reddeppa received his PhD in Physics, Chungnam Nat. Univ., Republic of Korea in August 2019. He is currently working as a Postdoctoral Fellow at Chungnam National University, Republic of Korea. His current research interests include synthesis and characterization of III-nitride semiconductor materials for optoelectronics and gas sensor applications.

Soyeon Ahn received the B.S. and M.S. degrees in Physics from Chungnam National University, Daejeon, Republic of Korea, in 2019 and 2021. She is currently a Ph.D. student at Chungnam National University in Department of Physics. Her current research interests are optical fiber sensors, gas sensors, and liquid crystals.

Youngseo Kim received his B.S. degree in Department of Physics from Chungnam National University, Daejeon, Republic of Korea, in 2021. He is currently a M.S. student in Department of Physics at Chungnam National University. His current studies include Side polished fiber base temperature sensors, Cholesteric liquid crystals and Fiber optical sensors.

Jong-Hyun Kim, received B.S. degree from Seoul National University, Korea, and M.S. and Ph.D. degrees from KAIST, Korea, respectively, all in physics. Currently he is a professor of department of Physics at Chungnam National University, Korea. His current research interests are liquid crystal alignment, colloid, and application.

Prof. Moon-Deock Kim received his Ph.D in department of semiconductor physics at Dongguk University, Republic of Korea in 1994. Currently he is professor of physics department at Chungnam Nat. Univ., Republic of Korea. His current research interests are Gas sensors, Photodetectors and III–V nitride semiconductor growth and device processing including LED'S, Solar cell and High Electron mobility transistors.

Seung Hee Lee received his B.S. degree in Physics from Jeonbuk National University, Republic of Korea in 1989 and Ph.D. degree from the Physics Department of Kent State University, USA in 1994. In 1995, he joined the LCD division at Hyundai Electronics. In the company, he invented and commercialized new liquid crystal devices, ‘‘Fringe-Field Switching (FFS)’’ mode which have become the main LC devices in highest resolution/performance LCDs. In September of 2001, he became a professor at Jeonbuk National University in Jeonju, Republic of Korea. He was awarded ‘‘SID Fellow’’ in 2008 and received the ‘‘Jan Rajchman Award’’ from SID in 2016. His main research fields are electro-optic materials and devices, and functional materials and sensors.

Prof. Min Yong Jeon (M′94) received the B.S. degree from Han Yang University, Seoul, Korea, in 1988, and the M.S. and Ph.D. degrees from Korea Advanced Institute of Science and Technology (KAIST), Daejeon, Korea, in 1990 and 1994, respectively, all in physics. He is currently a Professor in Department of Physics, Chungmam National University, Daejeon, Korea since May 2003. Prior to joining Chungnam National University, he worked in the area of optical router, as a Research Scientist at the University of California, Davis. From 1994–2001, he worked in the area of the optical network subsystem at the Electronics and Telecommunications Research Institute (ETRI), Daejeon, Korea. His current research interests include optical coherence tomography, wavelength swept laser, optical fiber sensors, and optical terahertz wave generation. Prof. Jeon is a Member of the IEEE, SPIE, OSA, KPS, and OSK.